Chapter 14

INTERVAL MODELLING, IDENTIFICATION AND CONTROL

As we have seen in earlier chapters, sharp and nonconservative estimates of robust stability margin and performance can be obtained for interval system models. Motivated by this, it is natural to attempt to model a family of uncertain systems using the interval framework. This chapter presents a such a technique. It consists of taking the frequency domain input and output data obtained from experimental test signals, and fitting an "interval transfer function" that contains the complete frequency domain behavior with respect to the test signals. Identification with such an interval model allows one to predict the worst case performance and stability margins using the results on interval systems given in the previous chapters. The algorithm is illustrated by applying it to experimental data obtained from an 18 bay Mini-Mast truss structure and a T-shape truss structure which are used in research on space structures.

14.1 INTRODUCTION

Obtaining a very accurate mathematical description of a system is usually impossible and very costly. It also often increases the complexity of the corresponding control mechanism. A recent trend in the area of system identification is to try to model the system uncertainties to fit the available analysis and design tools of robust control.

The interval transfer function described throughout this book is interpreted as a family of transfer functions whose coefficients are bounded by some known intervals and centered at the nominal values. In many cases this is unnatural in the sense that physical parameter perturbations do not correspond to transfer function coefficients. In order to relax this limitation, approaches to deal with linearly or multilinearly correlated perturbations have also been developed. On the other hand, if we observe

the developments in the interval system area we see that the *nominal system* has very little significance. These results in fact emphasize the *boundary properties* of the family of systems under consideration. In fact, virtually all the important results in this field are based on the boundary generating extreme points, edges, and segments of the interval family of systems.

With this background in mind, suppose that the behavior of the plant is described by some known test input and its corresponding measurement output. Due to noise, nonlinearities and inaccurate measurements, a fixed linear time-invariant identified model will never exactly represent the data obtained from the plant. Our aim, in this chapter, is to present an algorithm to obtain a reasonable interval transfer function model around, but not necessarily centered in, a nominally identified transfer function so that the entire frequency domain behavior of the physical plant is completely contained in that of the model.

This is applied to two experimental test structures. First, the algorithm is demonstrated by using the Mini-Mast truss structure. In this example, we show how to construct an interval transfer function model from the experimental data set. The frequency response of the resulting interval transfer function contains that of the experimental structure. For the second example, an interval transfer function is constructed to capture sets of experimental data that represent structural changes due to various added masses. Once the corresponding interval transfer functions are obtained, they are verified via the frequency domain analysis techniques described in Chapter 8 as well as their performance based on root locations described in Chapter 6.

In the next section, a simple technique is described. This technique deals with a single set of experimental data and constructs an interval transfer function which represents a reasonably small family containing the experimental data set.

14.2 INTERVAL MODELING WITH A SINGLE DATA SET

Consider the configuration shown in Figure 14.1.

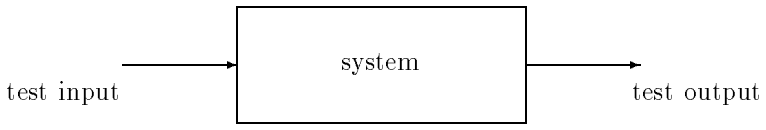

Figure 14.1. Experimental structure

In system identification, one applies test inputs and measures the system response in order to identify the parameters of an appropriate proposed mathematical model. It is also common that these test signals are represented in the form of frequency domain data. In fact, there are numerous techniques available to determine

a best possible linear time-invariant model that closely fits this frequency domain data set. Suppose that the test frequencies are $\omega_1,\omega_2,\cdots,\omega_N$ and the complex numbers $u(j\omega_i),y(j\omega_i)$ denote in phasor notation the input-output pair at the frequency ω_i. Let

$$y(j\omega_i) := D(j\omega_i)u(j\omega_i), \quad i = 1,2,\cdots,N \tag{14.1}$$

denote the test data generated from an identification experiment. Suppose that $G^I(s)$ is the transfer function of a linear time-invariant system which is such that $G^I(j\omega)$ is closest to $D(j\omega)$ in some norm sense. In general it is not possible to find a single rational function $G^I(s)$ for which $G^I(j\omega_i) = D(j\omega_i)$ and the more realistic identification problem is to in fact identify an entire family $\mathbf{G}(s)$ of transfer functions which is capable of "explaining" or "validating" the data in the sense that for each data point $D(j\omega_i)$ there exists some transfer function $G_i(s) \in \mathbf{G}(s)$ with the property that $G_i(j\omega_i) = D(j\omega_i)$. The family $\mathbf{G}(s)$ can be parametrized in many alternative ways. For instance, an unstructured approach to describing $\mathbf{G}(s)$ using a normed algebra is to let each element $G(s)$ of $\mathbf{G}(s)$ be described as $G(s) = G^I(s) + \Delta G(s)$ where the norm $|\Delta G(s)| < \rho$. In such a case, the family $\mathbf{G}(s)$ is identified once $G^I(s)$ and ρ are determined. In general, the identification algorithm should also be efficient in the sense that the family $\mathbf{G}(s)$ that it produces should be ideally minimal among the set of all such families that explain the data. In the unstructured case described above, this translates to choosing a small value of ρ.

The objective here is to develop an identification algorithm in a framework where the family of linear time-invariant systems $\mathbf{G}(s)$ is obtained by letting the transfer function coefficients lie in intervals around those of the nominal $G^I(s)$. The identification requirement is that

$$D(j\omega_i) \in \mathbf{G}(j\omega_i) \qquad \text{for all} \quad \omega_i. \tag{14.2}$$

Let

$$G^I(s) := \frac{n_0 + n_1 s + n_2 s^2 + n_3 s^3 + \cdots + n_n s^n}{d_0 + d_1 s + d_2 s^2 + d_3 s^3 + \cdots + d_n s^n}. \tag{14.3}$$

We define

$$G(s) := \frac{\hat{n}_0 + \hat{n}_1 s + \hat{n}_2 s^2 + \hat{n}_3 s^3 + \cdots + \hat{n}_n s^n}{\hat{d}_0 + \hat{d}_1 s + \hat{d}_2 s^2 + \hat{d}_3 s^3 + \cdots + \hat{d}_n s^n} \tag{14.4}$$

and

$$\begin{aligned} \mathbf{G}(s) := \{G(s) : \hat{n}_i \in [n_i - \mathrm{w}_{n_i}\epsilon^-_{n_i}, n + \mathrm{w}_{n_i}\epsilon^+_{n_i}], \\ \hat{d}_i \in [d_i - \mathrm{w}_{d_i}\epsilon^-_{d_i}, d + \mathrm{w}_{d_i}\epsilon^+_{d_i}], \qquad \text{for all} \quad i\} \end{aligned} \tag{14.5}$$

where

$$\begin{aligned} \underline{\mathrm{w}} &:= \left[\mathrm{w}_{d_0} \cdots \mathrm{w}_{d_n}\ \mathrm{w}_{n_0} \cdots \mathrm{w}_{n_n}\right] \\ \underline{\epsilon}^+ &:= \left[\epsilon^+_{d_0} \cdots \epsilon^+_{d_n}\ \epsilon^+_{n_0} \cdots \epsilon^+_{n_n}\right] \\ \underline{\epsilon}^- &:= \left[\epsilon^-_{d_0} \cdots \epsilon^-_{d_n}\ \epsilon^-_{n_0} \cdots \epsilon^-_{n_n}\right]. \end{aligned} \tag{14.6}$$

The components of w are to be regarded as weights chosen *apriori* whereas the ϵ's are to be regarded as dilation parameters to be determined by the identification algorithm and the data $D(j\omega_i)$

Remark 14.1. Note that in the expression in (14.5) we use vectors $\epsilon_{n_i}^{\pm}$ and $\epsilon_{d_i}^{\pm}$ instead of a single ϵ. This setting allows n_i and d_i to not necessarily be the center point of the intervals in which $\hat{n}_i$ and $\hat{d}_i$, lie respectively. This flexibility is important to achieve the minimum possible size of the family $\mathbf{G}(s)$.

The requirements on the identified interval model $\mathbf{G}(s)$ become:

1) *Membership Requirement:* $D(j\omega_i) \in \mathbf{G}(j\omega_i)$, for all i.

2) *Size Requirement:* $\|\underline{\epsilon}^{\pm}\|$ as small as possible.

3) *Frequency Response Requirement:* the weights $\underline{w}$ must be chosen so that the frequency response of $\mathbf{G}(j\omega)$ is bounded as tightly as possible for every frequency.

Both size and frequency response requirements are crucial because uniformly smaller intervals do not necessarily map to smaller image sets or a smaller family. For example, slightly bigger intervals in higher order coefficients may result in much bigger image sets than those due to significantly larger intervals in lower order coefficients.

14.2.1 Interval System Modeling

As described above, the procedure is divided into two parts. First, we identify a linear time-invariant model $G^I(s)$ which represents the test data $D(j\omega)$ as closely as possible. A variety of algorithms are available in the system identification literature and any algorithm can be taken for this step. Here, a simple least squares based algorithm is described. Once the nominal model is obtained, then the tightest intervals around each coefficient of the nominal transfer function $G^I(s)$ should be created while satisfying the membership and frequency response requirements.

14.2.2 Nominal System Identification

First, a brief description of a standard least squares method to identify a nominal transfer function whose frequency response fits the given test data $D(j\omega_i)$ as closely as possible is given. An appropriate order of model may be determined by checking the singular values of the Hankel matrix generated from the impulse response data. Under the assumption that the data is noise free, the number of nonzero singular values determines the order of the system. The details are omitted here. Interested readers may refer to the references [3] and [122]. After determining the appropriate order, n, of the system, we let the nominal transfer function be

$$G^I(s) := \frac{n(s)}{d(s)}. \tag{14.7}$$

The nominal transfer function coefficients must be selected to minimize the following index:

$$\sum_{i=1}^{N} \left\{ W^I(j\omega_i) \{ \mathrm{Re}[D(j\omega_i)d(j\omega_i) - n(j\omega_i)] \}^2 + \{ \mathrm{Im}[D(j\omega_i)d(j\omega_i) - n(j\omega_i)] \}^2 \right\}. \tag{14.8}$$

This least square problem generates $2N$ linear equations for $2n$ unknown coefficients of the transfer function. The weight W^I may be selected by finding the minimum variance estimator of unknowns. Since the relative error in the valley parts of the frequency response is more significant than the one in the peak parts, it is in general necessary to assign high weights for the frequency ranges in the valley parts of the frequency response.

14.2.3 Weight Selection

As shown in (14.5), the size of the interval of variation for each coefficient of the family $\mathbf{G}(s)$ depends on w and ϵ. In this subsection we consider the problem of finding an appropriate set of weights $\underline{\mathrm{w}}$. The weight selection procedure is extremely important because inappropriate selection of weights may result in an unnecessarily large family. This results in a large image set in the complex plane at some frequencies, even though the intervals themselves may be small.

It is natural to think that a weight represents the average sensitivity of a coefficient of the nominal model with respect to the variation of data points. Thus, we establish the following reasonable algorithm for selecting weights.

Suppose the test data consists of N data points obtained at corresponding frequencies,

$$D(j\omega) := \{ D(j\omega_i) = \alpha_i + j\beta_i, \quad i = 1, 2, \cdots, N \}. \tag{14.9}$$

Let us define the l^{th} model set as follows:

$$G_l(j\omega) = \begin{cases} D(j\omega_i), & i = l \\ G^I(j\omega_i), & i = 1, 2, \cdots, l-1, l+1, \cdots, N \end{cases}$$

In other words, the model $G_l(j\omega)$ is identical to the nominal identified model $G^I(j\omega)$ with the l^{th} data point replaced by the l^{th} component of the test data $D(j\omega)$. Now we construct the l^{th} identified model, which we call $G_l^I(s)$, which is identified from the l^{th} data set $G_l(j\omega)$. Let

$$G_l^I(s) := \frac{n_0^l + n_1^l s + n_2^l s^2 + n_3^l s^3 + \cdots + n_n^l s^n}{d_0^l + d_1^l s + d_2^l s^2 + d_3^l s^3 + \cdots + d_n^l s^n} \tag{14.10}$$

and

$$\mathbf{p} := \begin{bmatrix} n_0 & n_1 & \cdots & n_n & d_0 & d_1 & \cdots & d_n \end{bmatrix}. \tag{14.11}$$

If we assume that $|G_l(j\omega) - G_l^I(j\omega)|$ is small, the sensitivity of the coefficients of

the nominal model with respect to variations in the l^{th} data point is described as

$$\frac{\partial \mathbf{p}}{\partial G^I(j\omega_l)} := \begin{bmatrix} |n_0 - n_0^l| \\ \vdots \\ |n_n - n_n^l| \\ |d_0 - d_0^l| \\ \vdots \\ |d_n - d_n^l| \end{bmatrix}. \tag{14.12}$$

Collecting the sensitivity of the coefficients of the nominal model with respect to the variation of all the data points, $l = 1, 2, \cdots, N$, we have

$$\frac{\partial \mathbf{p}}{\partial G^I(j\omega)} :=$$

$$\begin{bmatrix} \dfrac{\partial \mathbf{p}}{\partial G^I(j\omega_1)} \\ \dfrac{\partial \mathbf{p}}{\partial G^I(j\omega_2)} \\ \vdots \\ \dfrac{\partial \mathbf{p}}{\partial G^I(\omega_N)} \end{bmatrix} = \begin{bmatrix} |n_0 - n_0^1| & \cdots & |d_0 - d_0^1| & \cdots & |d_n - d_n^1| \\ |n_0 - n_0^2| & \cdots & |d_0 - d_0^2| & \cdots & |d_n - d_n^2| \\ \vdots & & & & \\ |n_0 - n_0^N| & \cdots & |d_0 - d_0^N| & \cdots & |d_n - d_n^N| \end{bmatrix}.$$

The weights are then defined as the average of these for each coefficient:

$$\begin{aligned} \underline{\mathrm{w}} &:= \frac{1}{N}\left[\textstyle\sum_{l=1}^N |n_0 - n_0^l|, \cdots, \sum_{l=1}^N |d_n - d_n^l|\right] \\ &:= \left[\mathrm{w}_{n_0}, \cdots, \mathrm{w}_{n_n}, \mathrm{w}_{d_0}, \cdots, \mathrm{w}_{d_n}\right]. \end{aligned} \tag{14.13}$$

Using this selected weight, we proceed to determine the intervals of the transfer function coefficients.

14.2.4 Interval System Identification

After determining an appropriate weight vector w, we need to find $\underline{\epsilon}^{\pm}$ to satisfy the given requirements. We now first consider the membership requirement. Recall the nominal system given in (14.3) and substitute $s = j\omega$, then we have

$$\begin{aligned} G^I(j\omega) &:= \frac{n(j\omega)}{d(j\omega)} \\ &= \frac{(n_0 - \omega^2 n_2 + \cdots) + j(\omega n_1 - \omega^3 n_3 + \cdots)}{(d_0 - \omega^2 d_2 + \cdots) + j(\omega d_1 - \omega^3 d_3 + \cdots)} \\ &:= \frac{n^{\text{even}}(\omega) + j n^{\text{odd}}(\omega)}{d^{\text{even}}(\omega) + j d^{\text{odd}}(\omega)}. \end{aligned} \tag{14.14}$$

Since the nominal model transfer function $G^I(s)$ cannot perfectly represent the data set $D(j\omega)$, we have the following relationships for a particular frequency w_i.

$$\begin{aligned} D(j\omega_i) &= \alpha_i + j\beta_i \approx G^I(j\omega_i) \\ &= \frac{n^{\text{even}}(\omega_i) + jn^{\text{odd}}(\omega_i)}{d^{\text{even}}(\omega_i) + jd^{\text{odd}}(\omega_i)}. \end{aligned} \tag{14.15}$$

The difference may be added to the coefficients of the nominal model as follows:

$$\begin{aligned} D(j\omega_i) &= \alpha_i + j\beta_i \\ &= \frac{(\hat{n}_0 - \omega_i^2\hat{n}_2 + \cdots) + j(w_i\hat{n}_1 - \omega_i^3 n_3 + \cdots)}{(\hat{d}_0 - \omega_i^2\hat{d}_2 + \cdots) + j(w_i\hat{d}_1 - \omega_i^3 d_3 + \cdots)} \end{aligned}$$

where $\hat{n}_i := n_i + \mathrm{w}_{n_i}\epsilon_{n_i}$ and $\hat{d}_i := d_i + \mathrm{w}_{d_i}\epsilon_{d_i}$ for all i. If we rewrite this in terms of a linear matrix equation, we have

$$A(\omega_i, \alpha_i, \beta_i)W\underline{\epsilon}^i = B(\omega_i, \alpha_i, \beta_i) \tag{14.16}$$

where

$$A(\omega_i, \alpha_i, \beta_i) :=$$

$$\begin{bmatrix} \alpha_i & -\beta_i\omega_i & -\alpha_i\omega_i^2 & \beta_i\omega_i^3 & \cdots & -1 & 0 & \omega_i^2 & 0 & -\omega_i^4 & 0 & \cdots \\ \beta_i & \alpha_i\omega_i & -\beta_i\omega_i^2 & -\alpha_i\omega_i^3 & \cdots & 0 & \omega_i & 0 & -\omega_i^3 & 0 & \omega_i^5 & \cdots \end{bmatrix} \tag{14.17}$$

$$W := \begin{bmatrix} \mathrm{w}_{d_0} & & & & \\ & \cdots & & & \\ & & \mathrm{w}_{n_0} & & \\ & & & \cdots & \end{bmatrix}$$

$$\underline{\epsilon}^i := \begin{bmatrix} \epsilon^i_{d_0} & \cdots & \epsilon^i_{d_n} & \epsilon^i_{n_0} & \cdots & \epsilon^i_{n_n} \end{bmatrix}$$

and

$$B(\omega_i, \alpha_i, \beta_i) :=$$

$$\begin{bmatrix} -\alpha_i(d_0 - \omega_i^2 d_2 + \omega_i^4 d_4 - \cdots) + \beta_i(\omega_i d_1 - \omega_i^3 d_3 + \omega_i^5 d_5 - \cdots) \\ +(n_0 - \omega_i^2 n_2 + \omega_i^4 n_4 - \cdots) \\ -\beta_i(d_0 - \omega_i^2 d_2 + \omega_i^4 d_4 - \cdots) - \alpha_i(\omega_i d_1 - \omega_i^3 d_3 + \omega_i^5 d_5 - \cdots) \\ +(\omega_i n_1 - \omega_i^3 n_3 + \omega_i^5 n_5 - \cdots) \end{bmatrix}.$$

Here we assume without loss of generality that $A(\omega_i, \alpha_i, \beta_i)$ has full row rank. Then the minimum norm solution $\underline{\epsilon}_i$ can be computed as

$$\underline{\epsilon}_i = A(\cdot)^T \left[A(\cdot)A(\cdot)^T\right]^{-1} B(\cdot). \tag{14.18}$$

After finding $\underline{\epsilon}_i$ for all $i = 1, 2, \cdot, N$, the intervals of the transfer function coefficients are determined as follows:

$$\epsilon^-_{n_k} := \min_i\{0, \epsilon^i_{n_k}\} \qquad \epsilon^+_{n_k} := \max_i\{0, \epsilon^i_{n_k}\} \tag{14.19}$$

$$\epsilon^-_{d_k} := \min_i\{0, \epsilon^i_{d_k}\} \qquad \epsilon^+_{d_k} := \max_i\{0, \epsilon^i_{d_k}\} \tag{14.20}$$

for all k. Clearly, the procedure guarantees the satisfaction of the three requirements given earlier. Once the interval model is obtained, various extremal properties of this model can used in assessing the performance of any proposed controllers. These would exploit the results on interval systems developed in earlier chapters.

In the next section, the technique is illustrated by applying it to a large space structure experimental facility developed at NASA's Langley Research Center.

14.3 APPLICATION TO A MINI-MAST SYSTEM

14.3.1 Model Description

The Mini-Mast system shown in Figure 14.2 is a 20.16 meter-long deployable truss located in the Structural Dynamics Research Laboratory at NASA Langley Research Center. It is used as a ground test article for research in the areas of structural analysis, system identification, and control of large space structures. The Mini-Mast was constructed from graphite-epoxy tubes and titanium joints by using precision fabrication techniques. The 102 measurements shown in Figure 14.2 were derived using 51 noncontacting displacement sensors distributed from Bay 2 through Bay 18. Three shakers are located circumferentially around the truss at Bay 9 and their locations are selected primarily to excite the low frequency modes below 10 Hz. There are two bending modes and one torsion mode in this low frequency range. These three modes are designed to be separated from the other frequency modes. The experimental data used in this example is obtained by using one displacement sensor output at Bay 9 from one input. In this example, we use the experimental data within the 45 [rad/sec] low frequency range with 180 frequency data points. This low frequency range covers the three low frequency modes described earlier. Figure 14.3 shows the frequency response test data.

14.3.2 Interval Model Identification

Using the weighted least squares method described earlier, we select $W^I(j\omega)$ shown in Figure 14.4 (Top). The identified model obtained is

$$G^I(s) = \frac{n_0 + n_1 s + n_2 s^2 + n_3 s^3 + n_4 s^4 + n_5 s^5}{d_0 + d_1 s + d_2 s^2 + d_3 s^3 + d_4 s^4 + d_5 s^5 + s^6}$$

where

$$\begin{array}{ll} n_0 = -5.78 \times 10^4 & d_0 = 2.96 \times 10^7 \\ n_1 = \ 5.88 \times 10^2 & d_1 = 2.15 \times 10^5 \\ n_2 = -8.74 \times 10^2 & d_2 = 1.10 \times 10^6 \\ n_3 = \ 0.073 & d_3 = 2.75 \times 10^3 \\ n_4 = -0.967 & d_4 = 2.21 \times 10^3 \\ n_5 = \ 3.48 \times 10^{-5} & d_5 = 2.58 \end{array}$$

The eigenvalues of the identified model transfer function are as follows:

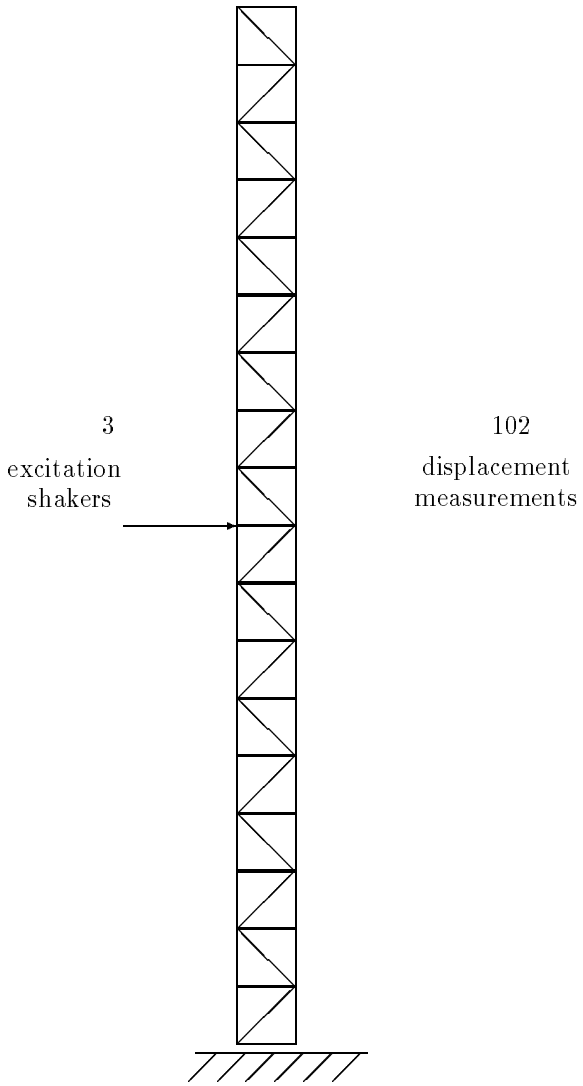

Figure 14.2. Mini-Mast structure

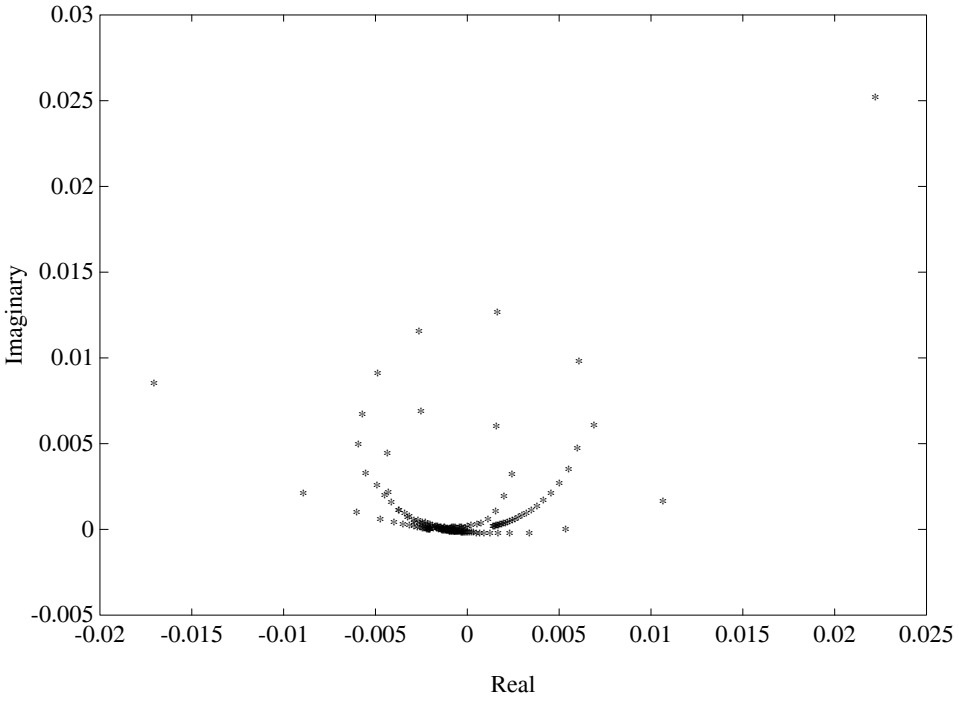

Figure 14.3. Experimental data set

	Eigenvalues	Mode
1	$-7.11 \times 10^{-2} \pm j5.3560$	1st bending mode
2	$-4.22 \times 10^{-1} \pm j26.302$	1st torsion mode
3	$-7.99 \times 10^{-1} \pm j38.616$	2nd bending mode

The magnitude and phase comparisons of the test data and the identified model are given in Figure 14.4 (Middle and Bottom). The dashed lines denote the frequency response of $D(j\omega)$ and the solid lines denote the frequency response of $G^I(j\omega)$. The dotted lines in Figure 14.4 (Middle) indicates the error in magnitude (i.e. $|D(j\omega) - G^I(j\omega)|$) for illustration.

We now create intervals around this nominal identified model. The weight selection method described in Section 14.2.3 gives the following weights for each coefficient:

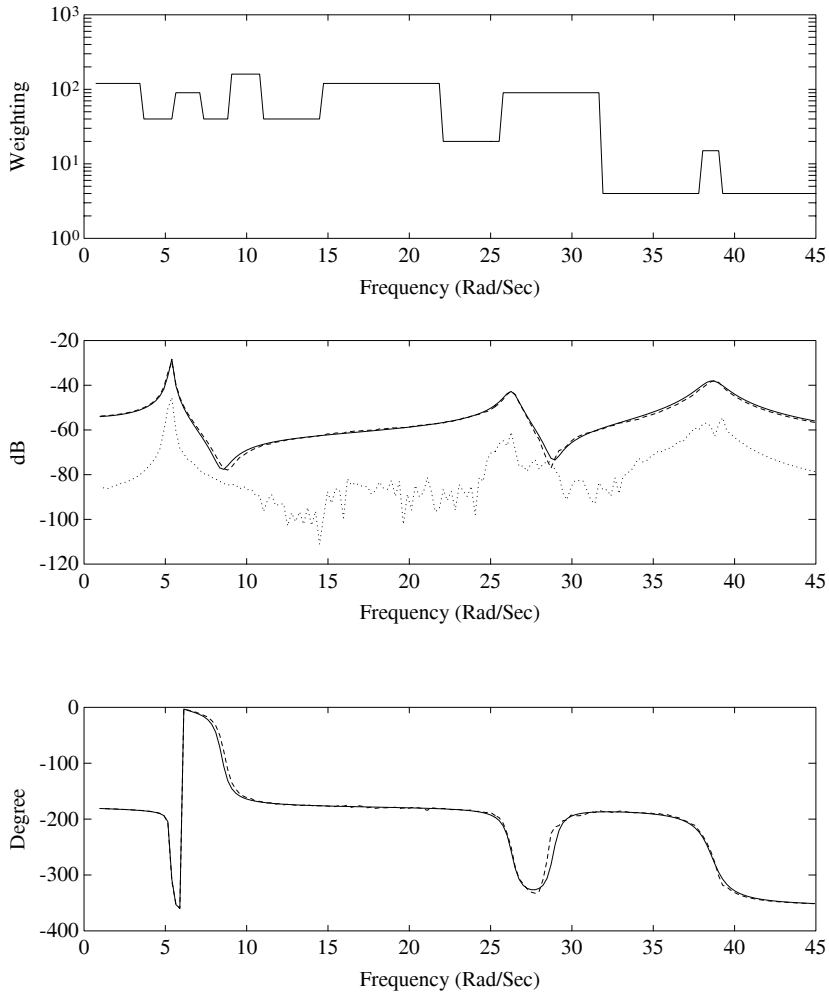

Figure 14.4. Least square weights (Top), Magnitude plots of identified model, experimental data, model error(Middle), Phase plots of identified model and experimental data (Bottom)

$$
\begin{aligned}
w_{n_0} &= 2.7053 \times 10 & w_{d_0} &= 3.9152 \times 10^{3} \\
w_{n_1} &= 1.2041 & w_{d_1} &= 2.2715 \times 10^{2} \\
w_{n_2} &= 2.3214 \times 10^{-1} & w_{d_2} &= 5.8095 \times 10 \\
w_{n_3} &= 4.0113 \times 10^{-3} & w_{d_3} &= 1.5250 \\
w_{n_4} &= 2.4768 \times 10^{-4} & w_{d_4} &= 5.9161 \times 10^{-2} \\
w_{n_5} &= 2.9620 \times 10^{-6} & w_{d_5} &= 1.2520 \times 10^{-3}
\end{aligned}
$$

This set of weights produced the following interval system:

$$\mathbf{G}(s) := \frac{\hat{n}_0 + \hat{n}_1 s + \hat{n}_2 s^2 + \hat{n}_3 s^3 + \hat{n}_4 + \hat{n}_5 s^5}{\hat{d}_0 + \hat{d}_1 s + \hat{d}_2 s^2 + \hat{d}_3 s^3 + \hat{d}_4 + \hat{d}_5 s^5 + s^6}$$

where

$$\begin{aligned}
\hat{n}_0 &\in [-6.006, -5.666]\times 10^4 & \hat{d}_0 &\in [2.936, 2.979]\times 10^7 \\
\hat{n}_1 &\in [\ 4.769,\ 7.840]\times 10^2 & \hat{d}_1 &\in [2.0663, 2.2335]\times 10^5 \\
\hat{n}_2 &\in [-8.959, -8.609]\times 10^2 & \hat{d}_2 &\in [1.092, 1.099]\times 10^6 \\
\hat{n}_3 &\in [-4.9791,\ 5.6904]\times 10^{-1} & \hat{d}_3 &\in [2.672, 2.841]\times 10^3 \\
\hat{n}_4 &\in [-9.749, -9.373]\times 10^{-1} & \hat{d}_4 &\in [2.209, 2.219]\times 10^3 \\
\hat{n}_5 &\in [-0.8570,\ 1.1648]\times 10^{-4} & \hat{d}_5 &\in [2.526, 2.619]\times 10^0
\end{aligned}$$

14.3.3 Model Validation

Figure 14.3 shows the polar plot of the test data for each frequency at which measurements were taken. Each mode of the polar plot has been separated in Figures 14.5(a), (b), (c) for illustration. The frequency envelope of the Interval Model is generated from the extremal segment set $\mathbf{G}_{\mathrm{E}}(s)$. These figures show that every data point of the test data is bounded by the image set generated by the interval model at the corresponding frequency. Figure 14.5(d) was drawn for the entire frequency range. These figures show that the uncertainty model obtained here is a valid interval model for the given test data set. Similarly, Figure 14.6 shows the magnitude and phase plots of the test data and the interval model. Clearly, both magnitude and phase plots of the test data are contained in the tightly bounded tubes representing the boundary of the frequency responses of the interval system.

In the next section another application is discussed. In this example, multiple data sets are used to identify the corresponding interval transfer function. Each data set represents the experimental structure with a specific set of added masses.

14.4 VIBRATION SUPPRESSION CONTROL OF A FLEXIBLE STRUCTURE

The objective of this example is to apply theoretical developments on interval systems to a laboratory experiment and to achieve meaningful robust control design and analysis of the vibration control problem of a flexible structure. Specifically, a controller is designed to damp structural vibrations such that changes in structural parameters can be tolerated. Therefore, it can be guaranteed that the level of damping will be bounded inside a predicted range.

The test structure is a scaled version of a typical flexible truss-like space structure and the parametric uncertainty is represented by mass added to various locations on the structure. This type of structural change is common in many space-bound dynamic systems. For example, appendage articulation or decreasing fuel weight over the life of a satellite are all possible system variations. While inertial changes were

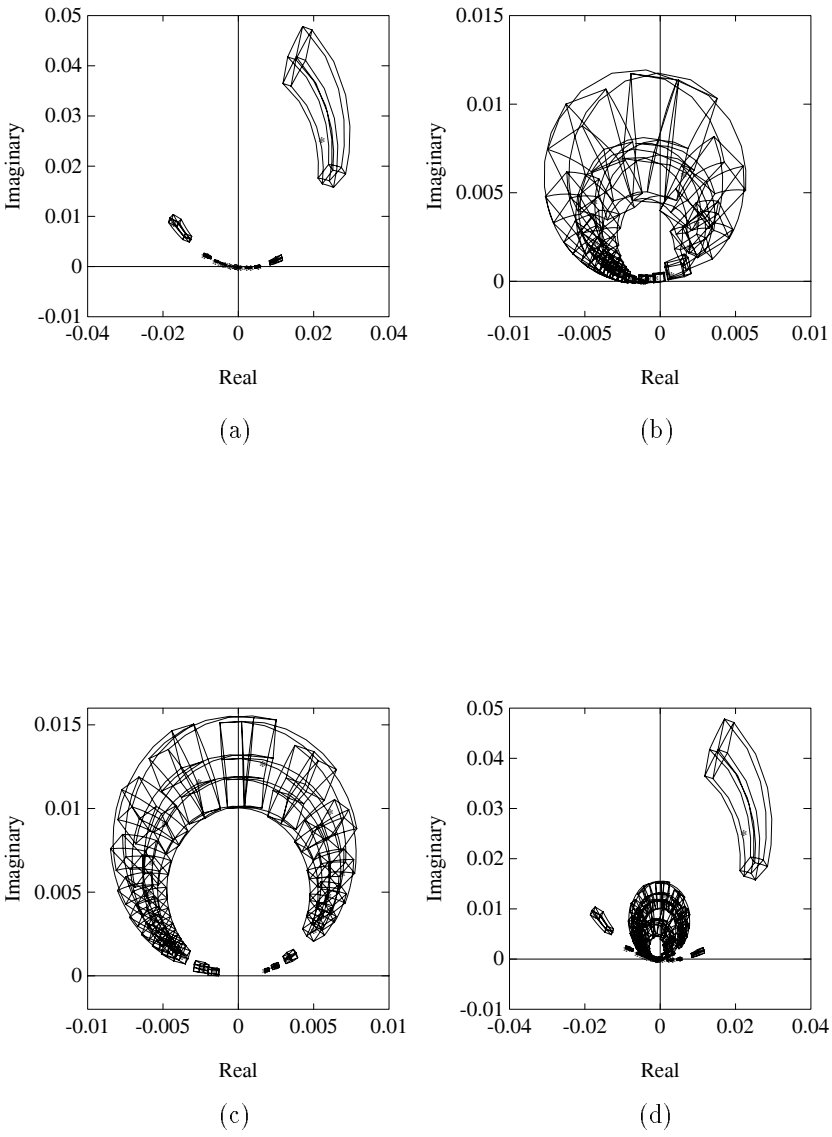

Figure 14.5. Nyquist images of interval model and experimental data (a) first mode, (b) second mode, (c) third mode, (d) image set of the system

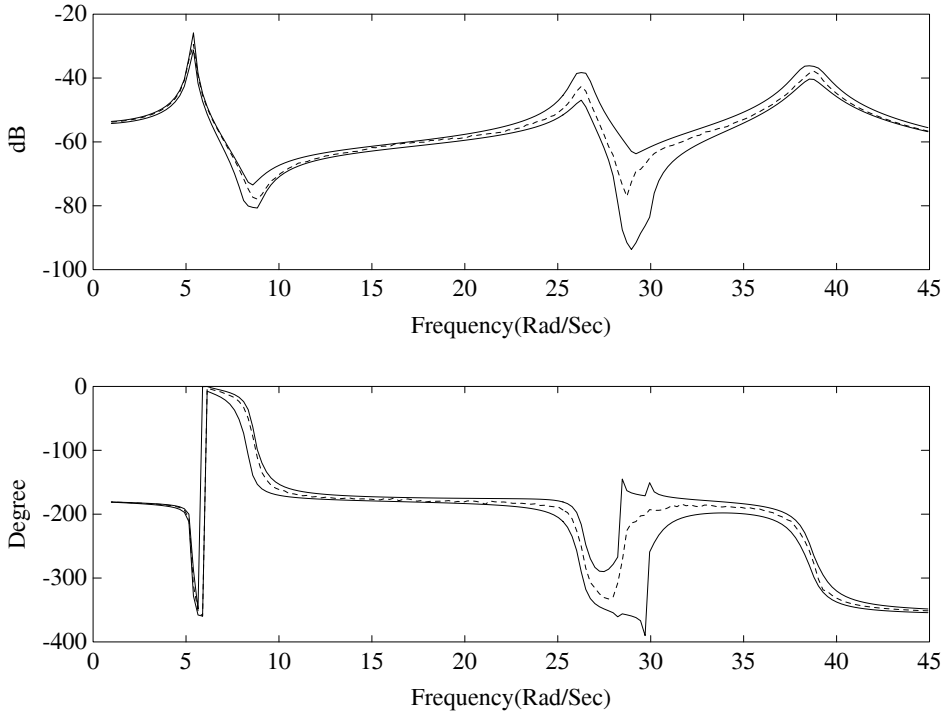

Figure 14.6. Bode plots of interval model and experimental data

chosen for this investigation, this by no means limits the methodology presented herein. Indeed, the effects of changes of any plant parameter, such as structural damping or moduli, could be accounted for in these interval system techniques. We start by describing the structural dynamics of the system.

Structural Dynamics

A 10-bay aluminum truss structure that was built for this experiment is shown in Figure 14.7. Each bay of the structure is a 0.5 meter cube made of hollow aluminum tubing joined at spherical nodes with threaded fasteners. The last three bays of the structure form a T-section. This is done so that the torsional modes of vibration will be more pronounced. The final structure has a mass of $31.5kg$ and is cantilevered horizontally from a massive monolithic base.

Figure 14.7. Ten Bay MeroForm Truss with T-section

A Finite Element Model (FEM) of the structure is shown in Figure 14.8. A modal analysis is performed on the model giving information about the structure's modal frequencies and mode shapes. The solution results in 7 modes of vibration in the 100Hz bandwidth. In order to establish the credibility of the model as well as embed

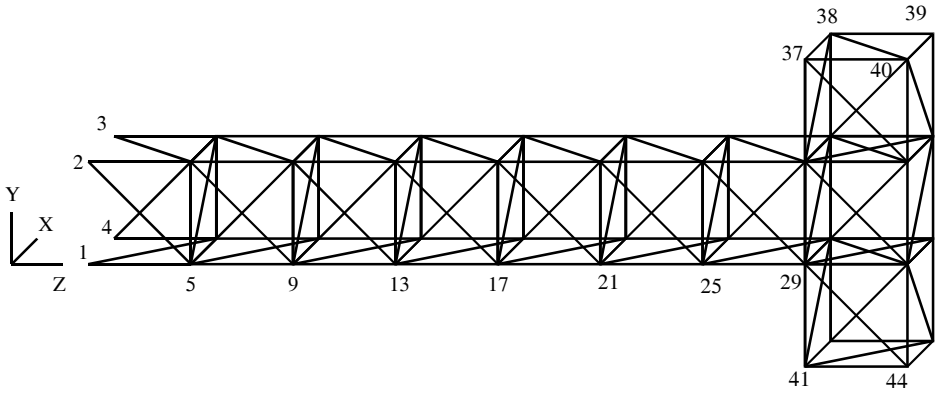

Figure 14.8. Finite element model of 10 bay truss including node number

natural structural damping data, experimental frequency domain data is collected from the structure using a Tektronix 2642A Fourier Analyzer. The input applied to the structure consists of an impulse applied to Node 40 (see Figure 14.8) of the structure, and the output is from an accelerometer mounted at Node 40 as well. The natural frequencies and damping ratios are extracted from the experimental data using the Eigensystem Realization Algorithm (ERA) method which we will not describe here. Interested readers may refer to reference [101]. Table 14.1 shows the resulting values for the first seven modes from the FEM model as well as the experimental data. From the FEM model we also extract a reduced-order mass matrix M and stiffness matrix K for the structure. The equation of motion for a multi-degree of freedom system is transformed into the standard modal form so that the modal damping matrix can easily be included. Transforming this back into physical coordinates yields the mass, stiffness, and damping matrices. Hence the following second-order lumped-mass parameter model of the structure was used to represent the structural dynamics.

$$M\ddot{x} + D\dot{x} + Kx = Bu \tag{14.21}$$

The vector x represents the physical coordinates of the structure, the vector u represents the force input into the structures, the triple (M, D, K) represents the

Table 14.1. Results of FEM model and ERA identified model

	Mode	FEM model	ERA model	
		Frequency(Hz)	Frequency(Hz)	Damping(ξ)
1	Vertical Bending	9.22	9.45	.0120
2	Horizontal Bending	9.31	9.70	.0140
3	Torsional	18.13	19.69	.0080
4	Vertical Bending	47.43	49.01	.0020
5	Horizontal Bending	55.12	60.30	.0010
6	Torsional	84.73	92.84	.0006
7	Mixed Motion	87.48	98.70	.0003

dynamics of the structure and the matrix B represents the input matrix. The damping matrix was developed from ERA identified modal parameters,

$$D = (S_m^T)^{-1} \Lambda_D S_m^{-1} \tag{14.22}$$

where

$$\Lambda_D = \text{diag}\,[2\xi_1 w_1, \ldots, 2\xi_n w_n]$$

and S_m is a mass normalized modal matrix for the reduced order model. The model represents a baseline model of the structure used in control design.

Actuator Dynamics

A reaction mass actuator (RMA) shown in Figure 14.9 is used to input force into the structure. This actuator uses a mass-magnet and electrical coil assembly to accelerate a proof-mass. An amplified signal applied to the stationary electrical coil creates a magnetic field. The constant field of the magnet inside the moving mass reacts against the new magnetic field causing force and hence movement of the mass. The mass rides on shafts which are limited to linear motion. The mass has a total usable travel length of about 2.5 cm. Any acceleration of the mass caused by force imparted from the coil results in an equal but opposite reaction force on the actuator's housing. When the actuator is mounted on the structure, the force is imparted on the structure. Hence, the actuator is space-realizable because it

requires no inertial reference frame such as the earth.

Figure 14.9. Reaction Mass Actuator assembly used for motion control

The actuator contains an internal non-contacting displacement sensor to aid in keeping the mass centered with respect to its housing. The block diagram of Figure 14.10 shows the local control scheme used for keeping the mass centered. The PD type controller contains a proportional feedback loop which acts as a spring and a derivative feedback loop which adds an equivalent viscous damping to the motion of the mass. The resulting system acts like a simple single degree of freedom mass-spring-damper system. Notice that a first-order filter is included to reduce the effects of high frequency noise in the damping loop. Realizing that the force output of the actuator is actually the inertial acceleration of the mass, the output force of the actuator has the following dynamics.

$$\frac{F(s)}{V_{\text{in}}(s)} = \frac{m\tau s^3 + ms^2}{m\tau s^3 + ms^2 + (c + k\tau)s + k} \tag{14.23}$$

where m is the reaction mass, k is the equivalent stiffness, c is the equivalent viscous damping constant, and τ is the time constant of the noise filter. This transfer

function represents the force output $F(s)$ with respect to the voltage input $V_{\text{in}}(s)$ applied to the RMA's coil, the output of the PD controller. As shown in Figure 14.7,

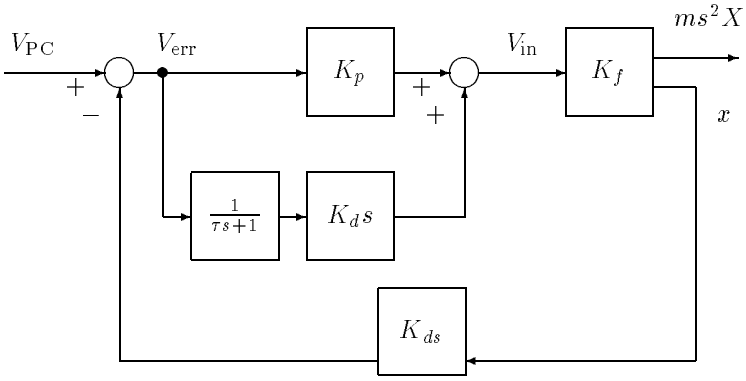

Figure 14.10. Block diagram of the local centering control system of RMA

the actuator is mounted between Node 39 and Node 40 of the structure. This location on the end of the structure is chosen because the modal participation factors of the first few modes of the structure are large at this location. A second-order model of the actuator and structure is created by combining the mass, stiffness, and damping coefficients of the actuator's local feedback system with the mass, stiffness, and damping matrices of the structure. This can be done when the constant τ is small enough that it doesn't have an effect in the frequency range of interest.

It should be noted that several design considerations were made when building an actuator and setting the local feedback gains. First, the actuator is designed so that its mass is small compared to the structure. The reaction mass is approximately 1.67 kg and the parasitic mass is $1.6kg$ so that the actuator is just over 10% of the structure's mass. Note also that the efficiency ratio of the actuator itself is 51%. The damping ratio of the actuator affects the damping in the structure both passively (without active control) and with the active control designed. These considerations were taken into account when choosing the internal damping in the actuator.

Parametric Uncertainty

The uncertainty of the structure considered here is due to masses added to Nodes 44 and 17. We want to examine the structural changes that occur when each added mass varies from 0kg to 2.5kg. In order to observe the frequency domain behaviour of the system with respect to the changes of these added masses, we take the following six samples of various weights of added masses as shown in Table 14.2. As

Table 14.2. 2 Masses Added to Structure

Case	1	2	3	4	5	6
Node 17	$0Kg$	$0.5Kg$	$1.0Kg$	$1.5Kg$	$2.0Kg$	$2.5Kg$
Node 44	$0Kg$	$0.5Kg$	$1.0Kg$	$1.5Kg$	$2.0Kg$	$2.5Kg$

a result, the modal frequencies are shifted as the masses are varied. Our particular interest is the model uncertainty for the first horizontal mode and the first torsional mode with the natural frequencies ranging 4 to 24Hz. The output measurement is from an accelerometer located at node 40 in the horizontal direction and the input is generated by applying the random signal to the RMA actuator. Figure 14.11 illustrates the change in the frequency peaks of the experimental data when these inertial parameters change.

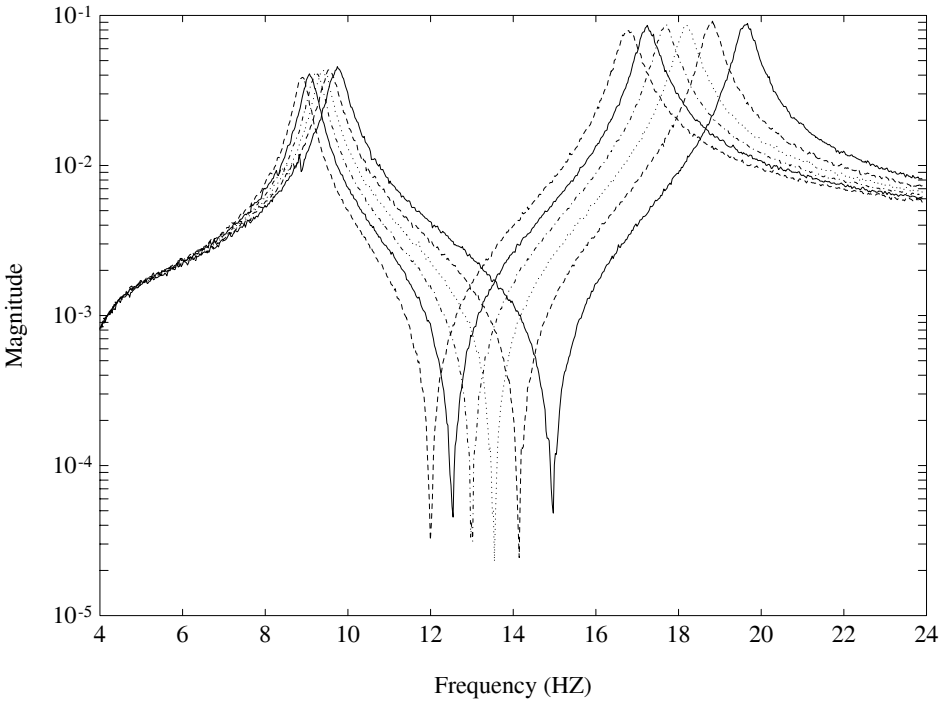

Figure 14.11. Experimental frequency response function with different added masses: From Right to Left $0Kg$, $1Kg$, $2Kg$, $3Kg$, $4Kg$, $5\ Kg$.

Therefore, it is reasonable to assume that for any value of added mass ranging 0 to 2.5 kg the frequency response of the corresponding structure remains inside the thinnest envelope covering the frequency response of these six sampled structures. By combining (14.21) and (14.23), we arrive at a transfer function expression of the actuator-structure composite system

$$G(s,p) = \frac{s^2 X(s,p)}{V_{\text{in}}(s)} \tag{14.24}$$

where $V_{\text{in}}(s)$ is the voltage across the actuator coils and $s^2X(s,p)$ is the response of an accelerometer. The unknown parameter, p, represents the uncertainty in the structural dynamics. Although we are using inertia to generate a family of perturbed systems, this by no means limits the techniques presented here to inertial perturbations only.

Vibration Suppression Control Law

The controller is designed using classical root locus techniques. Later it is cast in terms of interval control systems to observe the robustness of the closed loop system. Vibration damping is accomplished using a local velocity feedback (LVF) control scheme. Velocity feedback is fed into a single actuator from an accelerometer located at Node 40 horizontal direction, such that,

$$u = -K_v \dot{x}. \tag{14.25}$$

The control design is based on the model as in (14.21). Here we consider the model of the first horizontal bending mode and the first torsional mode. Feeding back the velocity term through feedback gain, K_v, the closed loop pole locations of the system are predicted. After varying the gain, a root locus plot is created. The resulting plot shows a trend of increased damping in all of the modes as the actuator gain increases. As expected, the actuator's damping is predicted to decrease and thus the pole of the actuator dominated mode moves toward the left half plane.

To implement the controller, a negative velocity signal is fed to the actuator to "cancel out" the motion of the structure, or reduce its velocity. An accelerometer is mounted on the housing of the actuator, and is thus connected to the structure. In order to get a velocity signal, the acceleration signal from the sensor must be integrated. However, integration of electrical signals results in exponential growth of any DC noise or DC offsets anywhere in the system. Therefore, we use a "velocity estimator" and the estimator is formulated as

$$\frac{\hat{V}(s)}{a(s)} = \frac{s}{s^2 + w_c s + w_c^2} \tag{14.26}$$

where w_c is the break frequency of the filter, $\hat{V}(s)$ is an estimated velocity signal and $a(s)$ is the accelerometer input. The value used here is $0.5Hz$, and since the

estimator acts like an ideal integrator at frequencies above $6w_c$, the feedback signal should be proportional to the velocity of the structure.

Initially, the controllers are implemented for the structural system with no added mass. Figure 14.12 shows the significantly increased damping in the first two modes(horizontal bending and torsional). The control is successful in increasing the system damping, but the question of robustness still remains unanswered. How much will slight changes in the system affect the closed loop control of the structure? The interval control model answers this question.

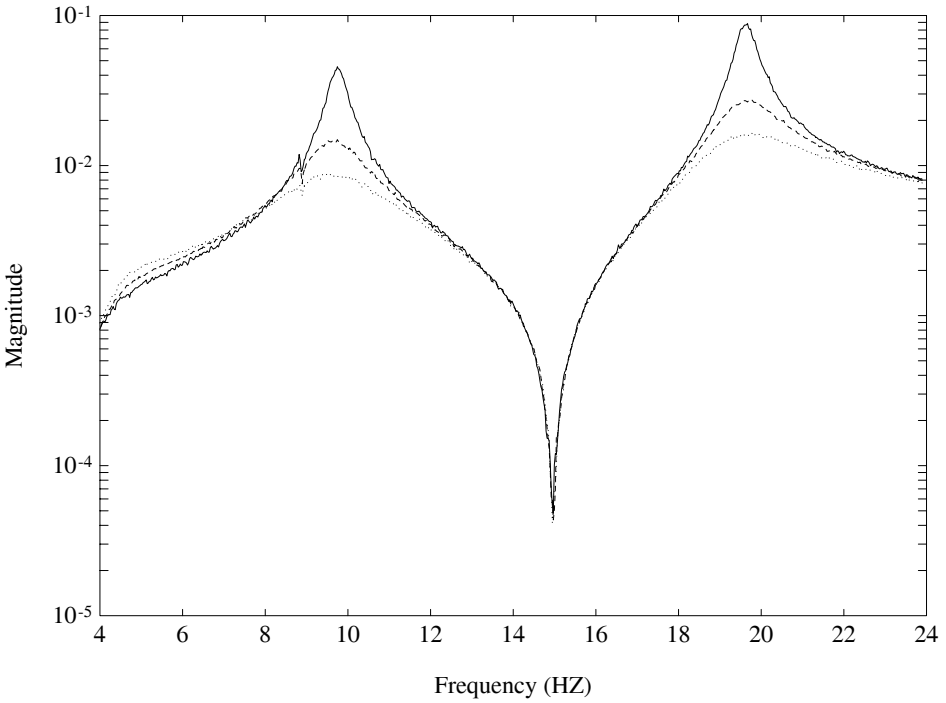

Figure 14.12. Experimental frequency response function of the open-loop and closed-loop systems with zero added masses: — Open-Loop; - - Closed-Loop $K_v = 30$; ... Closed-Loop $K_v = 60$.

14.4.1 Model Identification

Model Structure

The objective of this section is to construct a family of models such that its frequency response contains the six samples of experimental data shown in Figure 14.11. Each data set consists of 900 data points over the frequency ranging 4 to $24Hz$. We first

select the transfer function of the nominal model with an appropriate order:

$$\begin{aligned} g_0(s) &= \frac{n_0(s)}{d_0(s)} \\ &= \frac{n_m^0 s^m + n_{m-1}^0 s^{m-1} + \cdots + n_1^0 s + n_0^0}{s^m + d_{m-1}^0 s^{m-1} + \cdots + d_1^0 s + d_0^0} \end{aligned} \tag{14.27}$$

Here, we choose the structure of the family of transfer functions as follows:

$$\mathbf{G}(s) = \left\{ g(s) \;:\; \frac{n_0(s) + \sum_{i=1}^{m+1} \alpha_i r_i(s)}{d_0(s) + \sum_{j=1}^{m} \beta_j q_j(s)} \right\} \tag{14.28}$$

where $r_i(s)$ and $q_i(s)$ are base polynomials of degree m and $m-1$, respectively. The parameters α_i and β_i are the interval parameters which will be determined by their limiting values:

$$\alpha_i \in [\alpha_i^-, \alpha_i^+], \qquad \beta_i \in [\beta_i^-, \beta_i^+], \qquad \text{for all } \; i$$

Upon the determination of the interval family $\mathbf{G}(s)$, we expect that the frequency response of every structure corresponding to each and every value of added mass ranging over 0 to 2.5kg remains inside that of the family $\mathbf{G}(s)$.

In the next subsection we show how to determine the desired family of transfer functions $\mathbf{G}(s)$, equivalently determining a nominal model $g_0(s)$, a set of base polynomials $(r_i(s), q_i(s))$, and the limiting values of interval parameters α_i and β_i. We will call this type of model an *interval model*.

Interval Model Identification

The algorithm to generate an interval model starts with identifying a model for each sample set of data. Any standard identification technique can be used for this purpose and here we again use a least squares based system identification technique. We first determine the order of the transfer function:

$$\begin{aligned} g_i(s) &= \frac{n_i(s)}{d_i(s)} \\ &= \frac{n_m^i s^m + n_{m-1}^i s^{m-1} + \ldots + n_0^i}{s^m + d_{m-1}^i s^{m-1} + \ldots + d_0^i}, \qquad i = 1, \cdots, 6. \end{aligned} \tag{14.29}$$

Once a judicious choice of the order of the transfer function is made, determination of the coefficients of each transfer function may be found by solving a least square problem. Let $D_i(\omega)$ be the i^{th} sample data set consisting of 900 data points and $W(\omega)$ is a positive weighting function, then the least square solution generates the coefficient set of the transfer function $g_i(s)$, which minimizes the index:

$$J_i = \sum_{k=1}^{900} W(w_k) \left[R(\omega_k)^2 + I(\omega_k)^2 \right] \tag{14.30}$$

where

$$R(\omega_k) := \text{Real}\,[D_i(\omega_k)d_i(j\omega) - n_i(j\omega)]$$
$$I(\omega_k) := \text{Imag}\,[D_i(\omega_k)d_i(j\omega) - n_i(j\omega)]\,.$$

We repeat this procedure for all six test data sets to obtain the transfer functions $g_i(s)$, $i = 1, \ldots, 6$. A typical choice for the nominal model $g_0(s)$ is the average of these:

$$n_i^0 = \frac{1}{6}\sum_{k=1}^{6} n_i^k \qquad \text{and} \qquad d_i^0 = \frac{1}{6}\sum_{k=1}^{6} d_i^k. \tag{14.31}$$

The parameter perturbation vectors of the i^{th} identified model are defined as

$$\Delta n_i = n_i - n_0, \qquad \Delta d_i = d_i - d_0 \tag{14.32}$$

In order to determine the set of base polynomials $r_i(s)$ and $q_i(s)$ in (14.28), we employ a Singular Value Decomposition. To illustrate this SVD technique, we first form a matrix for the uncertainty of the denominator as

$$\Delta D = [\Delta \mathbf{d}_1 \;\; \Delta \mathbf{d}_2 \;\; \ldots \;\; \Delta \mathbf{d}_6]\,. \tag{14.33}$$

The SVD factors the matrix ΔD as

$$\Delta D = USV^T, \tag{14.34}$$

where U and V are orthonormal matrices and S is a rectangular matrix

$$S = [S_m \;\; 0] \tag{14.35}$$

with $S_m = \text{diag}[s_1,\ s_2,\ \ldots,\ s_m]$ and monotonically nonincreasing s_i, $i = 1, 2, \cdots, m$

$$s_1 \geq s_2 \geq \cdots \geq s_m \geq 0. \tag{14.36}$$

The number of non-zero singular values s_i is the rank of the matrix ΔD.

Suppose that the size of the perturbation matrix ΔD is $m \times n$ with $n \geq m$ and the number of the non-zero singular values is m_k. Then the corresponding coordinate vector of the perturbation $\Delta \mathbf{d}_i$ relative to this basis is

$$\Delta \mathbf{q}_i = U^T \Delta \mathbf{d}_i. \tag{14.37}$$

Thus, we have

$$\begin{aligned}[\Delta \mathbf{q}_1 \;\; \ldots \;\; \Delta \mathbf{q}_n] &= U^T\,[\Delta \mathbf{d}_1 \;\; \ldots \;\; \Delta \mathbf{d}_n] \\ &= U^T \Delta D.\end{aligned}$$

Here the singular value matrix is expressed as

$$S = \begin{bmatrix} S_{m_k} & 0 \\ 0 & 0 \end{bmatrix} = \begin{bmatrix} S^0_{m_k} \\ 0 \end{bmatrix} \tag{14.38}$$

with $S_{m_k} = \text{diag}\,[s_1,\ s_2,\ \ldots,\ s_{m_k}]$. Thus,

$$\begin{aligned}[\Delta\mathbf{q}_1\ \Delta\mathbf{q}_2\ \ldots\ \Delta\mathbf{q}_n] &= [\Delta\mathbf{d}_1\ \ldots\ \Delta\mathbf{d}_n] \\ &= U^T\Delta D \\ &= U^T U S V^T \\ &= U^T U \begin{bmatrix} S^0_{m_k} V^T \\ 0 \end{bmatrix} \\ &= I_m \begin{bmatrix} S^0_{m_k} V^T \\ 0 \end{bmatrix} \\ &= \begin{bmatrix} S^0_{m_k} V^T \\ 0 \end{bmatrix}\end{aligned}$$

where $S^0_{m_k} V^T$ is an $m_k \times n$ matrix. The last $m - m_k$ elements of any $\Delta\mathbf{q}_i$ are zero. From this, it is clear that all the uncertainty vectors $\Delta\mathbf{d}_i$ are inside the space spanned by the first m_k orthonormal vectors of U.

Furthermore, since $S^0_{m_k} V^T$ is of full rank, the dimension of the uncertainty matrix ΔD is m_k. Notice that the i^{th} $(i \le m_k)$ row vector of the matrix $[\Delta\mathbf{q}_1\ \ldots\ \Delta\mathbf{q}_n]$ is $s_i V_i^T$ with norm s_i. The j^{th} element of vector $s_i V_i$ represents the perturbation $\Delta\mathbf{d}_j$ in the direction of $\mathbf{u}_i$. Each singular value s_i indicates the magnitude of the perturbations in the direction of $\mathbf{u}_i$.

For structures with low damping, the scalar value d^0_0, which is the multiplicative product of the squares of all the natural frequencies, may be many orders larger than the scalar d^0_{m-1}, which is the sum of $2\xi_i w_i$ where ξ_i and w_i are the damping ratio and the natural frequency of the i^{th} mode, respectively. For example, we will show that d^0_0 of the first two modes in the model of the ten-bay structure is 10^7 times larger than d^0_3 of this model. Thus we need to compute the perturbation matrix with proper weights and we denote this weighted perturbation matrix as ΔD^W:

$$\Delta D^W = W_d^{-1}\Delta D \tag{14.39}$$

where $W_d = \text{diag}[w_d^1\ w_d^2\ \ldots\ w_d^m]$ and w_d^i is the standard deviation of the i^{th} row vector of ΔD. To find the distribution of the weighted uncertainty, we again use SVD to factor the matrix

$$\Delta D^W = U^W S^W (V^W)^T, \quad \text{where } U^W = [\mathbf{u}_1^W\ \ldots\ \mathbf{u}_m^W]. \tag{14.40}$$

Here the singular value s_i indicates the weighted perturbations distributed in the direction of $\mathbf{u}_i^W$. The corresponding coordinate vector of the uncertainty $\Delta\mathbf{d}_i^W$ relative to the basis $\{\mathbf{u}_1^W, \ldots, \mathbf{u}_m^W\}$ is

$$\Delta\mathbf{q}_i^W = (U^W)^T\Delta\mathbf{d}_i^W \tag{14.41}$$

Since the basis $\{\mathbf{u}_1^W, \ldots, \mathbf{u}_m^W\}$ corresponds to the weighted perturbation matrix ΔD^W, we want to find a basis corresponding to the nonweighted perturbation

matrix ΔD. From (14.39) and (14.40), the matrix ΔD can be written as

$$\Delta D = W_d U^W S (V^W)^T. \tag{14.42}$$

The basis for the nonweighted perturbation matrix ΔD is computed as

$$U_d = W_d U^W, \quad \text{where } U_d = [\mathbf{u}_{d1}\ \mathbf{u}_{d2}\ \ldots\ \mathbf{u}_{dm}] \tag{14.43}$$

The basis $\{\mathbf{u}_{d1}, \ldots, \mathbf{u}_{dm}\}$ for the nonweighted perturbation matrix ΔD is equivalent to the basis $\{\mathbf{u}_1^W, \ldots, \mathbf{u}_m^W\}$ for the weighted perturbation matrix ΔD^W. The corresponding coordinate vector of the uncertainty $\Delta \mathbf{d}_i$ relative to the basis $\{\mathbf{u}_{d1}, \ldots, \mathbf{u}_{dm}\}$ is

$$\begin{aligned} \Delta \mathbf{q}_i &= U_d^{-1} \Delta \mathbf{d}_i \\ &= (U^W)^{-1} (W_d)^{-1} (W_d) \Delta \mathbf{d}_i^W \\ &= (U^W)^T \Delta \mathbf{d}_i^W = \Delta \mathbf{q}_i^W. \end{aligned} \tag{14.44}$$

Notice that the nonweighted perturbation coordinate vector $\Delta \mathbf{q}_i$ is the same as the weighted coordinate vector $\Delta \mathbf{q}_i^W$. Both perturbation matrices therefore share the same singular values. The fixed polynomials $\mathbf{q}_i(s)$ of the interval model in (14.28) are now composed of the basis vectors of U_d,

$$\mathbf{q}_i(s) = \sum_{j=1}^{m} \mathbf{u}_{di}(j) s^{m-j} \tag{14.45}$$

where $\mathbf{u}_{di}(j)$ is the j^{th} element of vector $\mathbf{u}_{di}$. Finally, we determine the bounds for the corresponding polynomial $\mathbf{q}_j(s)$ as

$$\beta_j^+ = \max_{1 \le i \le 6} (\Delta \mathbf{q}_i(j)), \quad j = 1, \ldots, m \tag{14.46}$$

$$\beta_j^- = \min_{1 \le i \le 6} (\Delta \mathbf{q}_i(j)), \quad j = 1, \ldots, m \tag{14.47}$$

where $\Delta \mathbf{q}_i(j)$ is the j^{th} element of vector $\Delta \mathbf{q}_i$. This interval model represents an optimal linear box of the determined polynomials to cover the perturbation. Similarly, we also apply the SVD technique to the numerator perturbation matrix to obtain $r_i(s)$, α_i^-, and α_i^+.

The above procedure insures that each transfer function $g_i(s)$, $i = 1, 2, \cdots, 6$ that represents the system with different added masses is contained in the interval transfer function $\mathbf{G}(s)$. Consequently, we will be justified in carrying out design and analysis on this interval model.

14.4.2 Experimental Results

We utilize the techniques developed in Chapters 6 and 8 to analyze the vibration suppression control of the ten-bay truss structure with added mass uncertainty. A

reaction mass actuator(RMA) located between nodes 39 and 40 is used to excite and control the structure's motion. An accelerometer located at node 40 is used to measure the acceleration in the x direction at this position. Here we consider the model for the modes within the $4-24$ Hz frequency range. There are two modes, one bending mode and one torsional mode, in this bandwidth. The experimental frequency domain data were collected using a Tektronix 2642A Fourier Analyzer. The controller consists of a proportional-derivative (PD) system connected to the actuator. The transfer function of the actuator is denoted as $g_a(s)$, and we denote the transfer function of the actuator-structure composite system as $g_i(s)$. The 900 point frequency response functions of the experimental system with actuator dynamics (actuator-structure composite system) are expressed as

$$g_i(j\omega_k) = g_a(j\omega_k)g_i^0(j\omega_k), \quad k = 1, 2, \cdots, 900 \tag{14.48}$$

where g_i is the i^{th} set of experimental data and g_i^0 represents the system dynamics excluding actuator dynamics. The transfer function of the actuator is given by

$$\begin{aligned} g_a(s) &= \frac{n_a(s)}{d_a(s)} \\ &= \frac{2.3853 \times 10^{-3}s^3 + 1.6745s^2}{2.3853 \times 10^{-3}s^3 + 1.6745s^2 + 25.781s + 1251.3}. \end{aligned} \tag{14.49}$$

This includes the second order dynamics of the RMA, plus a first order filter used in conjunction with a PD controller which keeps the center of its mass positive at stroke. Following the modeling procedure described, we first apply the least squares technique to each set of data g_i^0 to obtain the identified model for each case of incremented added masses given in Table 14.2. Figure 14.13 compares the experimental data and the identified models including actuator dynamics. The figure shows that each identified model closely fits the corresponding experimental data set. The two peaks of each set of experimental data represent two structural modes and the natural frequency of each mode decreases when the added weight increases. Also the magnitude of each mode changes slightly for all the cases. Table 14.3 shows the structural eigenvalues of these six identified models. After we obtained the identified structural models excluding actuator dynamics, we computed the nominal model as the average of these six models and we have

$$\begin{aligned} g_0(s) &= \frac{n_0(s)}{d_0(s)} \\ &= \frac{-3.463 \times 10^{-3}s^4 - 1.173 \times 10^{-3}s^3 - 24.68s^2}{s^4 + 5.241s^3 + 16255s^2 + 40225s + 4.412 \times 10^7}. \end{aligned} \tag{14.50}$$

Recall the model structure in (14.28). If we determine the coefficients of the base polynomials $r_i(s)$ and $q_i(s)$, and intervals of the parameters α_i and β_i, the interval model will be completely determined. By applying the interval modelling procedure described in Section 14.4.1, the coefficients of these polynomials and intervals of the

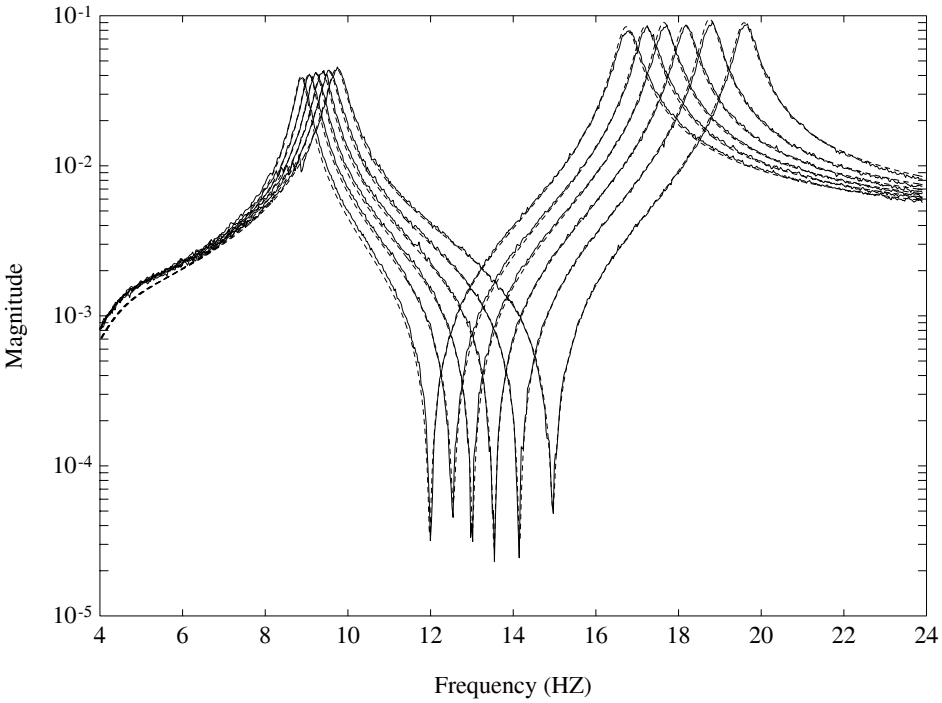

Figure 14.13. Experimental frequency response function (—) and Identified Models (- -): From Right to Left $0Kg$, $1Kg$, $2Kg$, $3Kg$, $4Kg$, $5\ Kg$.

Table 14.3. Eigenvalues of the identified models

Model No.	First mode	Second mode
1	-1.3864±j61.094	-1.4733±j123.00
2	-1.3065±j59.930	-1.3677±j117.76
3	-1.1854±j58.892	-1.4871±j113.96
4	-1.1081±j57.902	-1.4167±j110.79
5	-1.0424±j56.929	-1.4873±j108.03
6	-0.9581±j55.724	-1.5050±j105.10

parameters are obtained as shown in Tables 14.4 and 14.5. Table 14.4 shows that the coefficients of the denominator depicting the model uncertainty are dominated by the uncertainty in the direction of the first singular vector. The perturbation distributed in the direction of the fourth singular vector is around 1000 times smaller

Table 14.4. Coefficients of $q_i(s)$ and intervals of β_i

	$q_1(s)$	$q_2(s)$	$q_3(s)$	$q_4(s)$
s^3	1.4326×10^{-1}	-2.5118×10^{-1}	-1.8767×10^{-2}	-1.0399×10^{-3}
s^2	8.6678×10^{2}	5.5011×10^{2}	-8.0878×10^{2}	1.1301×10^{3}
s^1	4.1568×10^{3}	1.8545×10^{3}	6.8649×10^{3}	8.2205×10^{2}
s^0	4.0831×10^{6}	2.5353×10^{6}	-2.4265×10^{6}	-6.1023×10^{6}
β^+	3.1117×10^{0}	2.8036×10^{-1}	2.5123×10^{-2}	2.5140×10^{-3}
β^-	-2.3396×10^{0}	-2.1055×10^{-1}	-3.3913×10^{-2}	-2.5161×10^{-3}

Table 14.5. Coefficients of $r_i(s)$ and intervals of α_i

	$r_1(s)$	$r_2(s)$	$r_3(s)$	$r_4(s)$	$r_5(s)$
s^4	-8.7360×10^{-4}	-3.2529×10^{-5}	9.2234×10^{-5}	0	0
s^3	-1.3370×10^{-4}	3.8897×10^{-4}	1.0547×10^{-5}	0	0
s^2	-3.3372×10^{0}	-1.0513×10^{0}	-3.5316×10^{0}	0	0
s^1	0	0	0	1	0
s^0	0	0	0	0	1
α^+	2.4339×10^{0}	1.0485×10^{0}	6.3217×10^{-2}	0	0
α^-	-1.8816×10^{0}	-1.3450×10^{0}	-3.5834×10^{-2}	0	0

than that of the first singular vector. Table 14.5 shows that the model uncertainty of the numerator part is dominated by the uncertainty in the directions of the first two singular vectors. The Edge Theorem (Chapter 6) is now applied to the interval model obtained. Figure 14.14 shows the root clusters for two structural modes of interest. Experimentally identified eigenvalues are also included for comparison. From the interval model of the structure we obtained, we now can write the interval model of the system which includes the actuator dynamics (actuator-structure composite system), as follows:

$$G(s) = \frac{n_a(s)\left[n_0(s) + \sum_{i=1}^{m+1} \alpha_i r_i(s)\right]}{d_a(s)\left[d_0(s) + \sum_{i=1}^{m} \beta_i q_i(s)\right]}$$

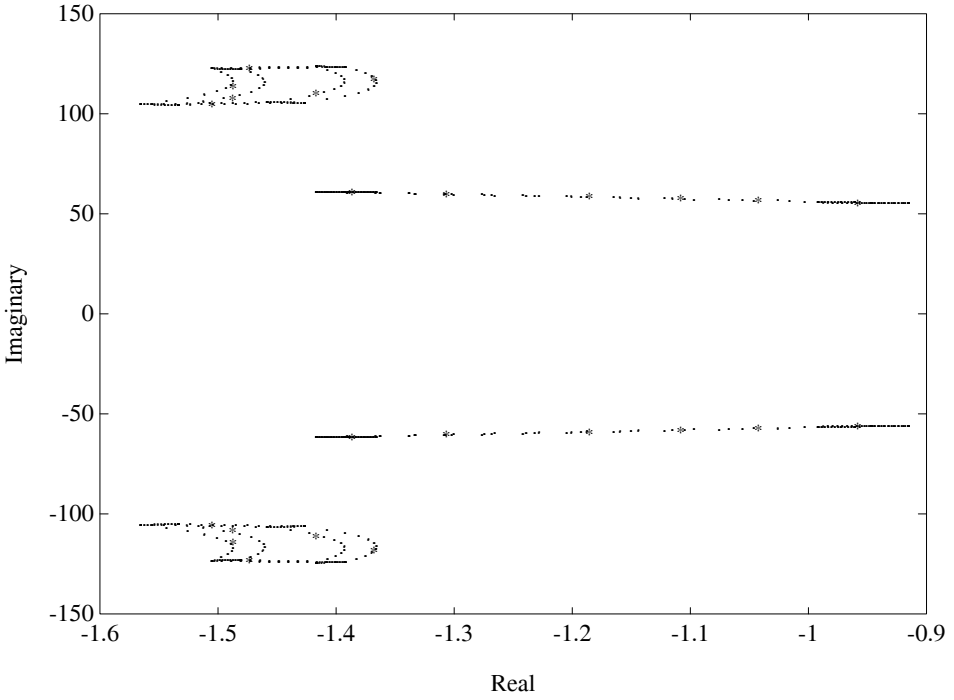

Figure 14.14. Root cluster (.) of closed-loop interval model and eigenvalues (*) of open-loop experimental structure for various added masses.

$$= \frac{n_a(s)n_0(s) + \sum_{i=1}^{m+1} \alpha_i n_a(s) r_i(s)}{d_a(s)d_0(s) + \sum_{i=1}^{m} \beta_i d_a(s) q_i(s)}. \tag{14.51}$$

Next, we apply the techniques described in Chapter 8 to obtain the magnitude envelopes of the interval model given in (14.51). Figure 14.15 shows the magnitude envelopes and the magnitude plots of the experimental transfer functions $g_i(\omega)$ for $i = 1, 2, \cdots, 6$. It is seen that the magnitude envelopes cover all the experimental data sets. It should be noted that these six experimental transfer functions represent a sample of all parametric changes which correspond to added masses at nodes 17 and 44. The interval model on the other hand accounts for the dynamics of the system for continuous changing masses at these two nodes up to $2.5Kg$. To verify the identified interval system by using the closed-loop experiment, we first design a local velocity feedback controller based on the root loci techniques for the vibration suppression of the structure. The transfer function of the controller is

$$K(s) = \frac{n_k(s)}{d_k(s)} = \frac{-110K_v s}{s^2 + \pi s + \pi^2}$$

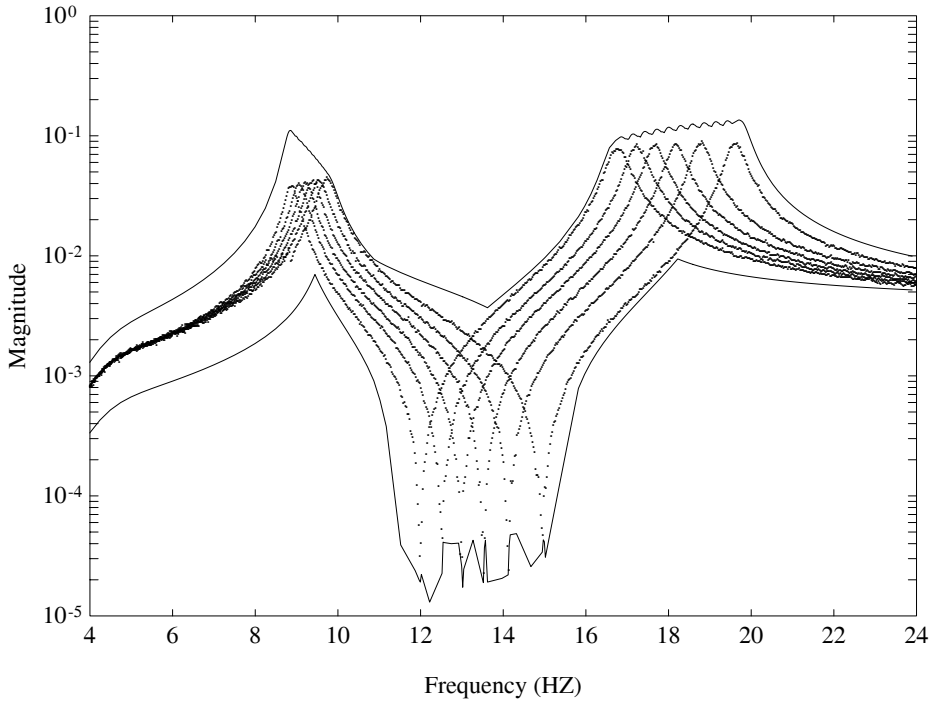

Figure 14.15. Magnitude envelope (—) of interval model and experimental data (..) for the open-loop system frequency response functions.

where K_v is the velocity feedback gain. The controller is designed for the structure without added masses. With $K_v = 30$, the damping ratio of the first mode is increased from 2.2% to 6.6% and the damping ratio of the second mode from 1.2% to 3.9%. The closed-loop interval system transfer function with the controller $K(s)$ can be computed as

$$T(s) = \frac{d_k(s)\left[n_a(s)n_0(s) + \sum_{i=1}^{m+1}\alpha_i(n_a(s)r_i(s))\right]}{d_k(s)\left[d_a(s)d_0(s) + \sum_{i=1}^{m}\beta_i(d_a(s)q_i(s))\right] + n_k(s)\left[n_a(s)n_0(s) + \sum_{i=1}^{m+1}\alpha_i(n_a(s)r_i(s))\right]}.$$

This interval system representation may be separated into the fixed and perturbation terms

$$T(s) = \frac{\alpha(s) + \sum_{i=1}^{m+1}\alpha_i\alpha_{1i}(s)}{\beta(s) + \sum_{i=1}^{m}\beta_i\beta_{1i}(s) + \sum_{i=1}^{m+1}\alpha_i\beta_{2i}(s)} \tag{14.52}$$

where the fixed part of the polynomials are

$$\alpha(s) = d_k(s)n_a(s)n_0(s),$$

$$\beta(s) = d_k(s)d_a(s)d_0(s) + n_k(s)n_a(s)n_0(s)$$

and the perturbation part polynomials are

$$\begin{aligned}\alpha_{1i}(s) &= d_k(s)n_a(s)r_i(s)\\ \beta_{1i}(s) &= d_k(s)d_a(s)q_i(s)\\ \beta_{2i}(s) &= n_k(s)n_a(s)r_i(s).\end{aligned}$$

Figure 14.16 depicts the magnitude envelope of the closed-loop interval system which shows that the envelope bounds the magnitude of the experimental transfer functions.

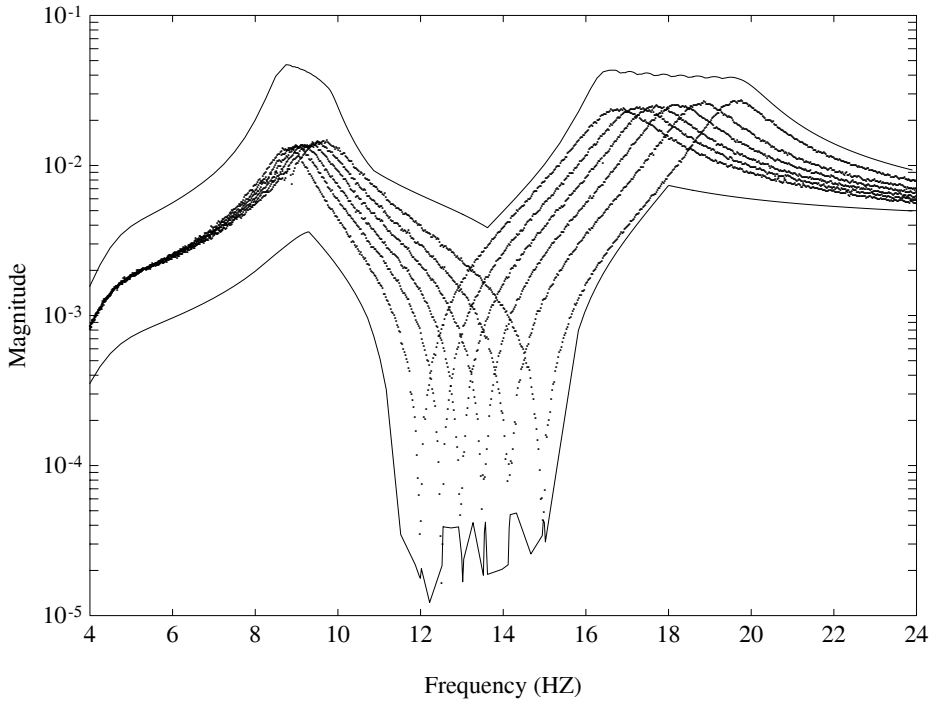

Figure 14.16. Magnitude envelope (—) of interval model and experimental data (..) for the closed-loop system frequency response functions.

The root clusters of the closed-loop interval system are also plotted by applying the Edge Theorem (Chapter 6) and it is given in Figure 14.17. The damping for each mode of the closed-loop family of systems is increased and this is verified by comparing the boundaries of the root clusters in Figures 14.14 and 14.17. Thus, from this root cluster plot, one can predict the worst case damping of the closed loop system while the added mass varies anywhere in between 0 to $2.5Kg$. In

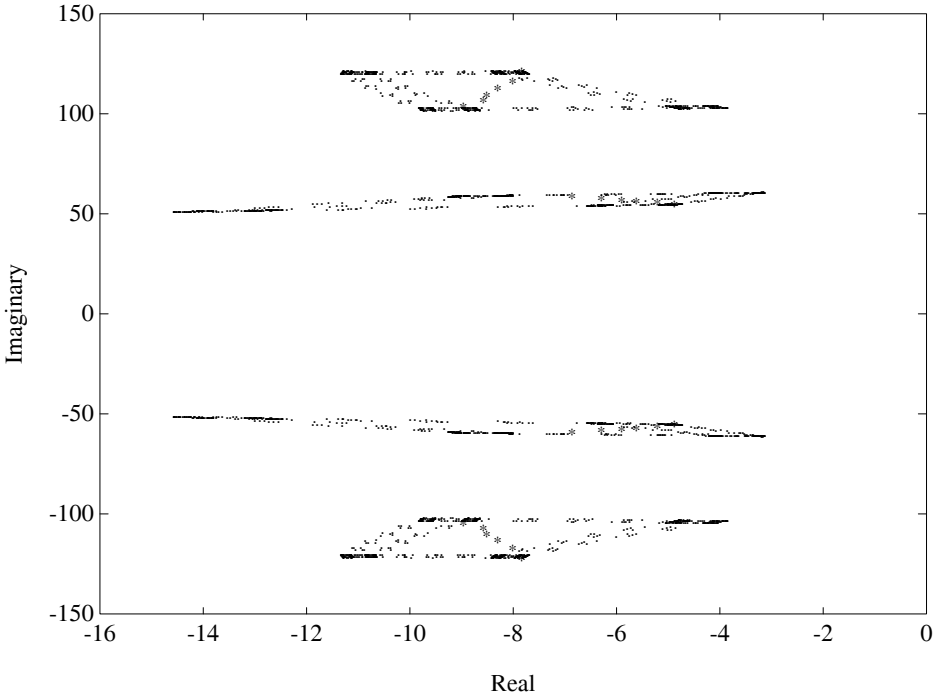

Figure 14.17. Root cluster (.) of closed-loop interval model and eigenvalues (*) of closed-loop experiment for $K_v = 60$.

other words, as long as the varied system remains inside the Bode envelope given in Figure 14.15, the poles of the closed loop system will remain inside the cluster regions shown in Figure 14.17.

14.5 NOTES AND REFERENCES

In this chapter we have freely employed a variety of terms used to explain system identification and the control structure experiment. We intentionally did not explain these terms in detail because our emphasis lies in interval system identification. However, the interested reader may refer to the following references for further details. An excellent collection of papers dealing with the issue of system identification and robust control is to be found in Kosut, Goodwin and Polis [151], [1], and references therein. These are mainly focused on the H_∞, ℓ_1 and μ problems. The least square approach used in Section 14.2.2 to determine a nominal linear time-invariant transfer function is described in detail by Adcock [3] and also by Juang and Pappa [122]. The method of selecting the normalized least square weight $W^I(j\omega)$ and its effect on the identified model are discussed in Bayard, Hadaegh,

Yam, Scheid, Mettler, and Milman [24]. They also discussed the problem of selecting an appropriate order of the transfer function in detail. The MATLAB ToolBox for Eigensystem Realization Algorithm (ERA) which was used to extract the natural frequencies and damping ratios from the experimental data for the second example was developed by Juang, Phan and Horta [123]. The details of the Reaction Mass Actuator (RMA) can be found in the work of Garcia, Webb and Duke [102]. The details of a Local Velocity Feedback (LVF) scheme which was used to accomplish vibration damping can be found in Zimmerman, Horner and Inman [248]. A velocity estimator is also described in Hallauer and Lamberson [107]. The first experiment was developed by Keel, Lew and Bhattacharyya [140]. The experiment was also modified to reflect mixed H_∞ and parametric uncertainty, and various results are reported in Lew, Keel and Juang [161, 162]. The second experiment was performed by Lew, Link, Garcia and Keel [163] and the related results are reported in Link, Lew, Garcia and Keel [164]. Different approaches of interval system modeling are also reported by Sotirov and Shafai [209] and [217].